Search for a time-dependent Z' resonance in the dimuon channel

Marlon P. Brade,[1,2,3,*] Jeremiah Juevesano,[2,4,3] Venus Abbegaile S. Carbonel,[2,3] Karen E. Bustamante,[2,3] Dennis C. Arogancia,[2] and Jan Mickelle V. Maratas[2,3]

[1]*Department of Physics, Western Mindanao State University–Main, Zamboanga City, Philippines*
[2]*Department of Physics, Mindanao State University–Iligan Institute of Technology, Iligan City, Philippines*
[3]*Mindanao Radiation Physics Center, Premier Research Institute of Science and Mathematics, MSU-Iligan Institute of Technology, Iligan City, Philippines*
[4]*Department of Mathematics, Physics, and Computer Science, University of the Philippines–Mindanao, Davao City, Philippines*

(Received 16 June 2026; accepted 25 September 2026; published 27 October 2026)

We present a time-domain search strategy for resonances with periodically varying masses in high-energy collider data. Conventional resonance searches rely on time-integrated event samples and are therefore insensitive to signals whose properties evolve during data taking. To address this limitation, we developed a two-dimensional unbinned likelihood framework in invariant mass and event time, allowing time-dependent resonances to be identified through characteristic trajectories in the (m, t) plane rather than as stationary peaks in the invariant-mass distribution. As a benchmark scenario, we consider a Z' boson arising from a gauged $U(1)_{B-L}$ extension of the Standard Model and introduce a phenomenological model in which the mediator mass undergoes periodic temporal modulation. The resulting signal produces distinctive correlations between invariant mass and event time that are not accessible to conventional time-integrated analyses. The method is applied to dimuon events from the CMS Open Data corresponding to the Run G data-taking period at $\sqrt{s} = 13$ TeV, with an integrated luminosity of 7.54 fb^{-1}. No statistically significant excess above the background-only hypothesis is observed for any of the benchmark time-dependent signal scenarios considered. Accordingly, 95% confidence level upper limits are derived on the signal production cross section and the corresponding gauge coupling $g_{Z'}$ as a function of the Z' mass for several benchmark values of the modulation amplitude. The resulting limits demonstrate that incorporating temporal information can enhance sensitivity relative to conventional time-integrated searches, particularly in the low- and intermediate-mass regions where sufficient signal statistics are available.

DOI: 10.1103/w7cw-b316

I. INTRODUCTION

The Standard Model (SM) of particle physics has achieved remarkable success in describing fundamental particles and their interactions. Nevertheless, it does not account for several established phenomena, including the nature of dark matter, the origin of neutrino masses and oscillations, the hierarchy problem, and the matter-antimatter asymmetry of the Universe [1–3]. Among these open questions, the nature of dark matter remains one of the central challenges in modern physics. Its existence is firmly established through multiple lines of astrophysical and cosmological evidence, including Galactic rotation curves, gravitational lensing, large-scale structure formation, and precision measurements of the cosmic microwave background [4]. However, its particle identity remains unknown, and no experiment to date has achieved a definitive direct or indirect detection. A broad experimental program has been developed to probe possible interactions between dark matter and the SM, including underground direct-detection experiments, beam-dump and fixed-target facilities, astrophysical observations, and high-energy collider searches [5–17]. In particular, collider and intensity-frontier experiments have explored a wide range of portal scenarios connecting dark matter to visible matter, yet no confirmed signal has been observed. This persistent absence of evidence motivates the exploration of alternatives beyond the traditional weakly interacting massive particle (WIMP) paradigm, including axions, sterile neutrinos, and particles residing in hidden or dark sectors [18–22].

Among these possibilities, ultralight bosonic dark matter has attracted significant interest due to its distinctive

*Contact author: marlon.brade@g.msuiit.edu.ph

Published by the American Physical Society under the terms of the Creative Commons Attribution 4.0 International license. Further distribution of this work must maintain attribution to the author(s) and the published article's title, journal citation, and DOI. Funded by SCOAP³.

wavelike behavior on macroscopic scales [23]. For sufficiently small masses, the large occupation number allows it to be described as a coherent classical field rather than a collection of individual particles. This field undergoes oscillations with a frequency set by its mass and can remain coherent over astrophysical timescales. Such behavior arises naturally in scenarios where the dark matter abundance is generated via the misalignment mechanism. A direct consequence is the possibility of inducing time-dependent effects in particle physics observables, leading to signatures that are not captured by conventional time-integrated searches. These time-varying phenomena provide a complementary avenue for probing dark matter interactions. The possibility that ultralight scalar dark matter induces time-dependent modulations of collider observables has been explored in previous studies [24–26]. In the present work, we consider the specific scenario in which the coherent oscillation of the scalar field induces a periodic modulation of the effective mediator mass, giving rise to characteristic time-dependent signatures at collider experiments.

In this work, we extend this framework to the case of a Z' gauge boson associated with a gauged $U(1)'$ symmetry, in which the mediator couples directly to a conserved SM current. While the underlying mechanism of mass modulation remains similar, the phenomenology differs due to the distinct coupling structure and production channels. In particular, we focus on a Z' boson arising from a gauged $U(1)_{B-L}$ extension of the SM, which provides a well-motivated benchmark [27–29]. A key feature of this scenario is that the signal does not appear as a stationary resonance in invariant mass, but instead evolves in time, tracing a trajectory in the (m, t) plane. As a result, conventional analyses that rely on time-integrated invariant mass distributions may significantly dilute the signal, especially for large modulation amplitudes. To address this, we develop a time-domain search strategy based on a two-dimensional likelihood in invariant mass and time. This approach retains the correlation between these observables and allows for the direct reconstruction of the time-dependent signal.

Although the analysis is presented in the context of the $B-L$ model, the methodology is formulated at the level of collider observables and is therefore applicable to a broader class of scenarios involving time-dependent mediator properties. The analysis is performed using dimuon events from the CMS Open Data corresponding to an integrated luminosity of 7.54 fb^{-1} collected during the 2016 Run G data-taking period [30,31]. Run G spans approximately 26.5 days and provides event-by-event GPS timestamps, allowing the likelihood to be constructed directly as a function of the event time. The observed event-time distribution is incorporated explicitly through the time-dependent normalization procedure described in Sec. II, thereby accounting for the nonuniform detector exposure and data-taking rate throughout the run. Run G was selected because it provides a substantial integrated luminosity together with an observational window sufficiently long to probe the benchmark oscillation periods considered in this work. Although the proposed methodology is, in principle, applicable to multiple CMS data-taking periods, extending the analysis beyond a single period introduces additional experimental and statistical considerations. In particular, successive data-taking periods may be separated by substantial intervals with no recorded collisions, even though the hypothesized signal evolves continuously in time.

A. Model

We consider an extension of the SM by an additional Abelian $U(1)'$ gauge symmetry with gauge boson Z'_μ. The present analysis is formulated within a low-energy effective field theory in which the heavy degrees of freedom responsible for the spontaneous breaking of the $U(1)'$ symmetry have been integrated out. Consequently, the Z' mass is treated as an effective low-energy parameter originating from the heavy symmetry-breaking sector, while the present work focuses on the collider phenomenology arising from its time-dependent modulation. Although renormalizable portal interactions between the heavy symmetry-breaking scalar and the dark matter field are generally allowed, we consider the regime in which such couplings are sufficiently suppressed that their contributions to the low-energy phenomenology can be neglected.

The effective Lagrangian is given by

$$\mathcal{L} = -\frac{1}{4} Z'_{\mu\nu} Z'^{\mu\nu} + \frac{1}{2} m^2_{0Z'} Z'_\mu Z'^\mu + g_{Z'} Z'_\mu J^\mu_{Z'}, \qquad (1)$$

where $Z'_{\mu\nu} = \partial_\mu Z'_\nu - \partial_\nu Z'_\mu$, $g_{Z'}$ denotes the $U(1)'$ gauge coupling, and $J^\mu_{Z'}$ is the corresponding fermionic current. The dark matter sector consists of a complex scalar field ϕ carrying $U(1)'$ charge Q_ϕ. The ultralight scalar mass m_ϕ is treated as an effective low-energy parameter, while its UV origin and stabilization mechanism are assumed to arise from physics above the effective theory. Accordingly, the present analysis should be regarded as an effective description valid at the energy scales relevant to collider phenomenology. The homogeneous dark matter field evolves according to

$$\ddot{\phi} + 3H\dot{\phi} + m^2_\phi \phi = 0, \qquad (2)$$

where H is the Hubble expansion rate. At late times, the field undergoes coherent classical oscillations with the approximate solution

$$\phi(t) \simeq \phi_0 \cos(m_\phi t + \delta), \qquad (3)$$

where ϕ_0 is the oscillation amplitude and δ is the phase of the oscillation. The interaction between the dark matter field and the $U(1)'$ gauge boson arises through the covariant derivative

$$D_\mu\phi = (\partial_\mu - ig_{Z'}Q_\phi Z'_\mu)\phi, \tag{4}$$

which generates the interaction

$$|D_\mu\phi|^2 \supset (g_{Z'}Q_\phi)^2|\phi|^2 Z'_\mu Z'^\mu. \tag{5}$$

Within the effective theory, the coherent oscillating dark matter background modifies the effective mass of the Z' according to

$$m^2_{Z'}(t) = m^2_{0Z'} + (g_{Z'}Q_\phi)^2|\phi(t)|^2. \tag{6}$$

Substituting the oscillatory solution into Eq. (6) gives

$$m^2_{Z'}(t) = m^2_{0Z'} + (g_{Z'}Q_\phi)^2\phi_0^2\cos^2(m_\phi t + \delta). \tag{7}$$

Factoring out the constant mass scale yields

$$m^2_{Z'}(t) = m^2_{0Z'}\left[1 + \frac{(g_{Z'}Q_\phi)^2\phi_0^2}{m^2_{0Z'}}\cos^2(m_\phi t + \delta)\right]. \tag{8}$$

It is therefore convenient to define the dimensionless modulation parameter

$$\kappa \equiv \frac{(g_{Z'}Q_\phi)^2\phi_0^2}{m^2_{0Z'}}, \tag{9}$$

which measures the amplitude of the dark-matter-induced mass modulation. The effective Z' mass can then be written compactly as

$$m^2_{Z'}(t) = m^2_{0Z'}(1 + \kappa\cos^2(m_\phi t + \delta)). \tag{10}$$

Equation (10) forms the basis of the phenomenological analysis presented in this work. The four parameters $\{m_{0Z'}, \kappa, m_\phi, \delta\}$ completely specify the time-dependent evolution of the resonance mass within the effective description considered here. Interference between the time-dependent Z' signal and the SM background is not considered in the present phenomenological treatment. A consistent treatment of such effects, including their possible time dependence arising from the varying Z' mass, requires a dedicated amplitude-level theoretical analysis and is left for future work.

II. METHODOLOGY

In this work, we develop a time-dependent search strategy for a neutral vector boson Z' in scenarios where its effective mass is modulated by a coherently oscillating ultralight scalar background. This leads to a phenomenology that differs substantially from conventional resonance searches, where the signal is assumed to appear as a stationary peak in invariant mass distributions. In the present scenario, the resonance mass evolves in time, producing a signal with a nontrivial structure in the joint invariant mass-time plane. Consequently, analyses based solely on time-integrated invariant mass spectra can significantly dilute the signal, particularly when the modulation amplitude is large and the resonance sweeps across a broad mass range. To retain sensitivity to this behavior, we construct a two-dimensional likelihood in the observable space (m, t), where $m \equiv m_{\mu\mu}$ is the dimuon invariant mass and t is the event time. The signal probability density function (PDF) is explicitly defined in this two-dimensional space, allowing the correlation between invariant mass and time to be treated directly within the likelihood. Unlike standard bump hunts, where sensitivity arises from localized excesses in invariant mass, the signal considered here appears as a time-dependent trajectory in the (m, t) plane. Preserving this structure is therefore essential, motivating the use of a fully unbinned likelihood that maximizes the information retained from the data.

A. Signal and background probability distribution function

The analysis is performed in the two-dimensional observable space defined by the invariant mass m and event time t. Figure 1 shows the invariant mass distribution of the selected dimuon events together with the fitted background model. Good agreement is observed over the full mass range considered in the analysis, including both the resonant Z-boson peak and the nonresonant Drell-Yan continuum at higher masses.

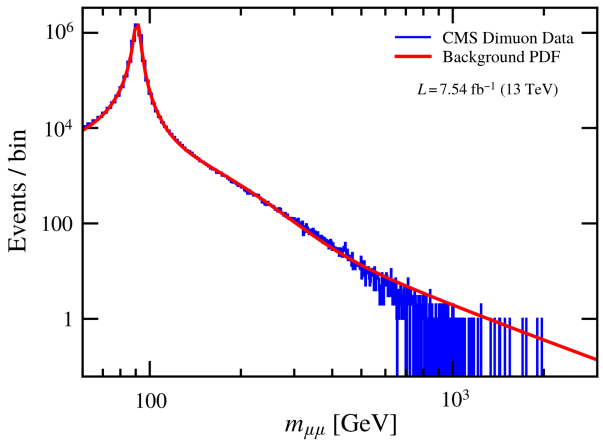


FIG. 1. Invariant mass distribution of dimuon events together with the fitted background model. The data are well described across the full mass range, including the Z-boson resonance and the smoothly falling high-mass tail. The fit is performed using an extended unbinned likelihood.

The signal PDF is constructed to describe the time-dependent evolution of the Z' resonance mass induced by the oscillating scalar-field dark matter background. At a fixed time, the reconstructed invariant-mass distribution is modeled by a Gaussian function,

$$S(m,t) = \frac{1}{\sqrt{2\pi}\sigma_{\mathrm{res}}} \exp\left[-\frac{(m-\mu(t))^2}{2\sigma_{\mathrm{res}}^2}\right], \qquad (11)$$

where σ_{res} denotes the detector mass resolution. The resulting two-dimensional signal PDF in the invariant mass and time variables is illustrated in Fig. 2, while the corresponding time-integrated signal PDF is shown in Fig. 3. Throughout this analysis, the resolution is parametrized as $\sigma_{\mathrm{res}} = 0.01 m_0$. For the low-mass region, $50 \le m_0 \le 120$ GeV, a value of $\sigma_{\mathrm{res}} = 0.02 m_0$ is adopted. In the vicinity of the Z-boson resonance, the large Standard Model background, together with a narrow signal parametrization, makes the evaluation of the expected upper limits numerically challenging. The broader signal parametrization is therefore adopted only in this mass region to ensure a stable likelihood evaluation.

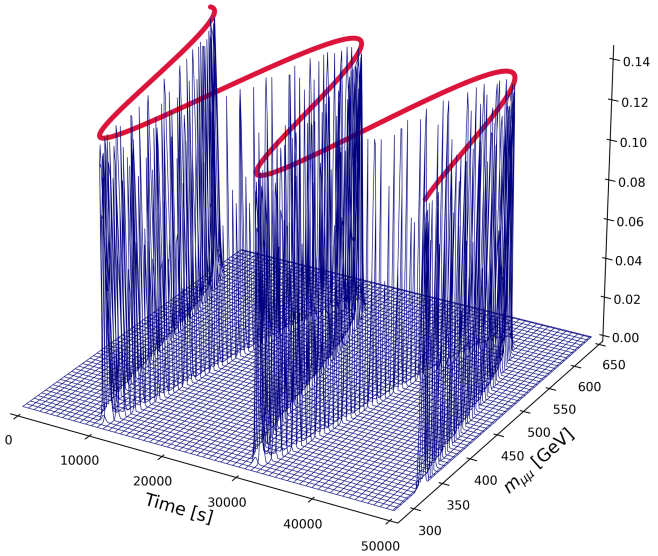


FIG. 2. Time-dependent evolution of the mass component of the signal PDF, $S(m,t)$, for the benchmark point $m_0 = 300$ GeV, $\kappa = 3$, and $\tau = 20660$ s. The Gaussian resonance follows the time-dependent mean $\mu(t)$. The time-dependent acceptance function $T(t)$ is applied separately in the full signal PDF used in the likelihood.

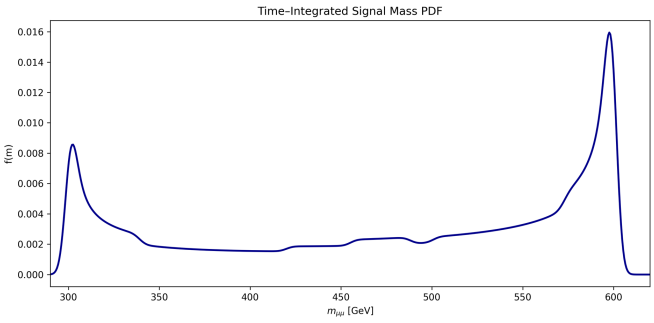


FIG. 3. Time-integrated signal mass probability density function obtained by integrating the two-dimensional signal template $S(m,t)$ over the full Run G data-taking period. The distribution is shown for the benchmark point $m_0 = 300$ GeV and $\kappa = 3$.

The time-dependent mean of the resonance is parametrized as

$$\mu(t) = m_0 \sqrt{1 + \kappa \cos^2\left(\frac{\pi t}{\tau} + \delta\right)}, \qquad (12)$$

where m_0 is the nominal resonance mass, κ controls the modulation amplitude, τ is the oscillation period, and δ is an arbitrary phase offset. This parametrization provides a minimal phenomenological description of a resonance whose mass undergoes periodic modulation due to the coherent oscillation of the scalar dark matter field. Consequently, the signal exhibits a nonfactorizable correlation between invariant mass and event time, which constitutes the characteristic experimental signature exploited in the present analysis.

Throughout this work, we consider a benchmark scalar mass of $m_\phi \simeq 10^{-19}$ eV, corresponding to an oscillation period of $\tau \simeq 20660$ s (≈5.7 hours). This benchmark is particularly well suited for the present analysis because the modulation is neither sufficiently rapid to be washed out by the finite event statistics nor sufficiently slow to sample only a small fraction of an oscillation cycle during the data-taking period. Instead, multiple oscillation cycles are expected to occur over the CMS Run G dataset while retaining adequate statistics within each cycle to reconstruct the evolving resonance structure. Furthermore, the coherence time of an ultralight scalar field with this mass is expected to greatly exceed the duration of the dataset, allowing the modulation to be treated as a coherent periodic signal throughout the analysis. To account for variations in detector exposure throughout the data-taking period, the signal probability density function is multiplied by a time-dependent acceptance function $T(t)$, as follows:

$$P_{\mathrm{sig}}(m,t) = S(m,t)T(t). \qquad (13)$$

The background contribution is modeled as the sum of two components corresponding to resonant Z-boson production and the nonresonant Drell-Yan continuum,

$$P_{\mathrm{bkg}}(m,t) = P_Z(m,t) + P_{\mathrm{DY}}(m,t). \qquad (14)$$

The resonant Z-boson contribution is modeled using a double-sided Crystal Ball (DCB) function, which describes the Gaussian core together with asymmetric non-Gaussian tails arising from detector resolution effects and final-state radiation. The DCB shape parameters are fixed using CMS

Open Data simulation samples [32]. The nonresonant Drell-Yan contribution is modeled using a log-curved power-law function,

$$B_{\mathrm{DY}}(m) \propto m^{-(n+b\log m)}, \tag{15}$$

which provides a flexible parametrization of the smoothly falling invariant-mass spectrum over the full search region.

Both background components are multiplied by the common time-dependent acceptance function $T(t)$, shown in Fig. 4. The acceptance function is constructed from individual CMS run numbers, where each run corresponds to a contiguous data-taking period during which the detector configuration, calibration constants, trigger menu, and operating conditions remain approximately stable. For each run i, spanning the time interval $[t_i^{\min}, t_i^{\max})$, the acceptance is assigned the value

$$T(t) = \frac{N_Z^{(i)}}{\Delta t_i}, \qquad t \in [t_i^{\min}, t_i^{\max}), \tag{16}$$

where $N_Z^{(i)}$ denotes the number of reconstructed $Z \to \mu^+\mu^-$ candidates satisfying

$$80\ \mathrm{GeV} < m_{\mu\mu} < 100\ \mathrm{GeV}, \tag{17}$$

and

$$\Delta t_i = t_i^{\max} - t_i^{\min} \tag{18}$$

is the duration of the corresponding CMS run. Since the inclusive Z-boson production cross section is expected to remain constant during data taking, the observed Z-boson event rate provides a data-driven estimate of the effective detector exposure. Consequently, the acceptance function incorporates the combined effects of the average luminosity during each CMS run, detector acceptance, and data-taking efficiency, thereby providing a piecewise-constant description of the slowly varying detector exposure throughout the data-taking period.

The run-based construction of the acceptance function represents a physically motivated compromise between detector stability and statistical precision. Because detector configuration, calibration, trigger settings, and operating conditions are expected to remain approximately stable within a given CMS run, constructing the acceptance function on a run-by-run basis naturally preserves these periods of stable detector operation. In contrast, arbitrary fixed-width time intervals may span multiple CMS runs, thereby mixing data collected under different detector configurations or operating conditions into a single acceptance estimate. Conversely, substantially finer intervals, such as individual luminosity sections, contain significantly fewer Z-boson events and consequently lead to larger statistical fluctuations in the estimated detector exposure. Each CMS run therefore provides sufficient Z-boson statistics to obtain a stable and physically meaningful estimate of the relative detector exposure.

The acceptance function serves only as a normalization correction and does not determine the time resolution of the signal model. For each event, the signal probability density function is evaluated using the exact event timestamp through the time-dependent mean $\mu(t)$ defined in Eq. (12), while the corresponding value of $T(t)$ is

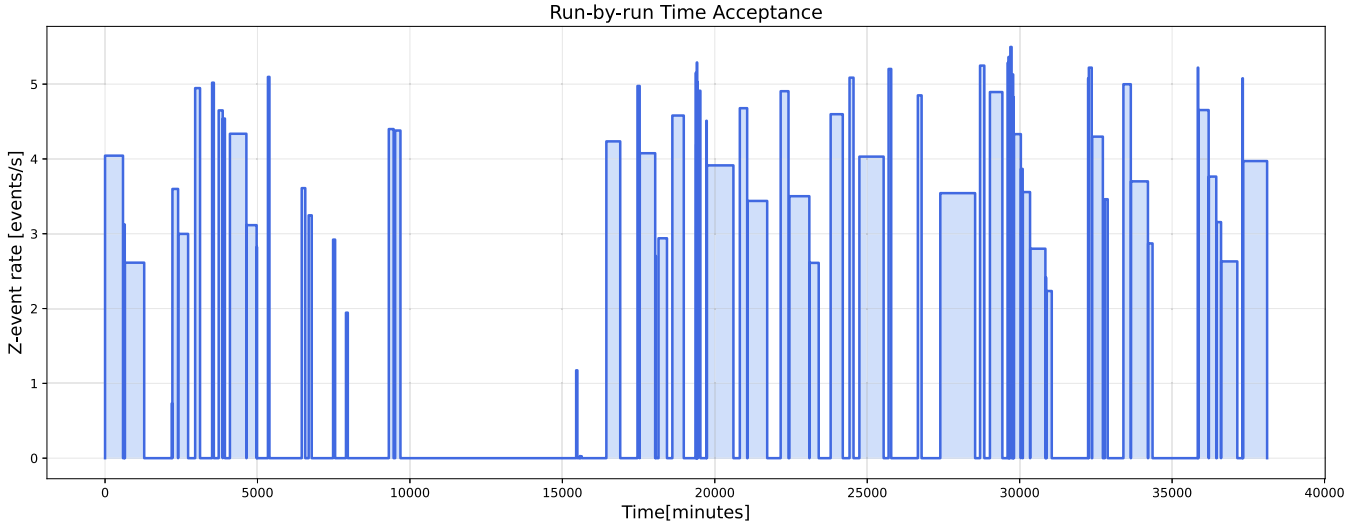


FIG. 4. Piecewise-constant time-dependent acceptance function derived from the CMS Run G Open Data. For each CMS run, the acceptance is computed as $N_Z/\Delta t$, where N_Z is the number of reconstructed $Z \to \mu^+\mu^-$ candidates satisfying $80 < m_{\mu\mu} < 100$ GeV and Δt is the duration of the corresponding run. The resulting function provides a data-driven estimate of the effective detector exposure, incorporating the combined effects of the average luminosity, detector acceptance, and data-taking efficiency, and is applied as the common time-dependent acceptance function for both the signal and background probability density functions.

determined solely by the CMS run in which the event was recorded. Consequently, the temporal evolution of the signal is treated continuously on an event-by-event basis, whereas the acceptance function corrects only for the slowly varying detector exposure and does not affect the continuous time evolution described by Eq. (12).

The background probability density functions are therefore written as

$$P_Z(m,t) = Z(m)T(t),$$
$$P_{\mathrm{DY}}(m,t) = B_{\mathrm{DY}}(m)T(t). \tag{19}$$

The complete likelihood is constructed as an extended model in which the signal and background yields are determined simultaneously from the fit. While the SM background factorizes into independent invariant-mass and time components through the common acceptance function, the signal remains intrinsically nonfactorizable owing to the time-dependent mean defined in Eq. (12). This correlation between invariant mass and event time constitutes the principal discriminating feature of the analysis, enabling a periodically varying resonance to be distinguished from SM backgrounds. The overall structure of the background model together with the observed event distribution in the (m,t) plane is illustrated in Fig. 5.

B. Statistical analysis

Statistical inference is performed using a modified frequentist approach based on the profile likelihood method [33,34]. The analysis employs an extended unbinned likelihood constructed in the two-dimensional observable space of invariant mass and event time, thereby preserving the full event-by-event information while comparing the signal and background hypotheses. The parameter of interest is the signal yield, N_{sig}. The background normalizations, N_Z and N_{pow}, are treated as nuisance parameters and are profiled during the likelihood maximization. All remaining model parameters are determined through auxiliary studies prior to the final hypothesis test and are subsequently fixed. The tail parameters of the double-sided Crystal Ball function (α_L, n_L, α_R, and n_R) are first determined from CMS Open Data simulation. These parameters are then fixed in a preliminary fit to the invariant-mass distribution of the data, in which the Z-boson peak position (μ_Z), detector mass resolution (σ_Z), the Drell-Yan shape parameters (n_{pow} and b_{pow}), together with the background normalizations (N_Z and N_{pow}), are allowed to vary. The resulting best-fit values define the background model used in the subsequent statistical analysis.

For each benchmark signal hypothesis, a preliminary two-dimensional fit is subsequently performed to determine the best-fit value of the signal phase δ. The fitted value of δ, together with the calibrated background shape parameters and the benchmark signal parameters (m_0, κ, and τ), is then fixed in the final profile likelihood. Consequently, the final statistical inference contains only three free parameters: the parameter of interest, N_{sig}, and the nuisance parameters, N_Z and N_{pow}. This reduces the dimensionality of the likelihood optimization while preserving the independently calibrated signal and background models. The profile likelihood ratio test statistic is defined as

$$q_\mu = -2\ln\left(\frac{\mathcal{L}(\mu,\hat{\hat{\theta}})}{\mathcal{L}(\hat{\mu},\hat{\theta})}\right), \tag{20}$$

where μ denotes the signal strength parameter, $\hat{\mu}$ and $\hat{\theta}$ are the values of the signal strength and nuisance parameters that globally maximize the likelihood function, and $\hat{\hat{\theta}}$ denotes the conditional maximum-likelihood estimator of the nuisance parameters for a fixed value of μ.

In the absence of a statistically significant deviation from the background-only expectation, upper limits are derived

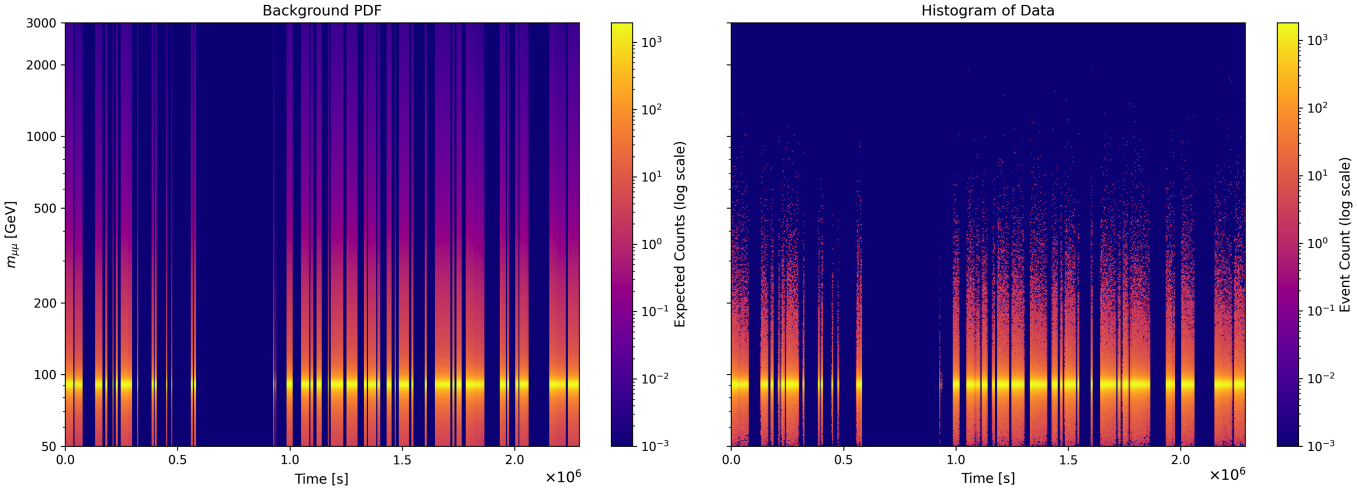


FIG. 5. Illustration of the background structure in the (m,t) plane.

using the CL_s prescription. Exclusion limits at the 95% confidence level (CL) are obtained for the signal hypothesis parametrized by μ, which in the present analysis corresponds to the product $\sigma(pp \to Z') \times \mathrm{BR}(Z' \to \mu^+\mu^-)$. Signal hypotheses satisfying $CL_s < 0.05$ are considered excluded at the 95% CL. In the event of a significant excess, the corresponding global significance would be evaluated while accounting for the look-elsewhere effect associated with the scan over the mass and modulation hypotheses considered in the analysis.

C. Determination of the $(M_{Z'}, g_{Z'})$ exclusion limits

The exclusion limits in the $(M_{Z'}, g_{Z'})$ parameter space are obtained by translating the expected 95% CL upper limits on the signal production cross section into constraints on the gauge coupling. For each benchmark mediator mass, the upper limit on $\sigma(pp \to Z') \times \mathrm{BR}(Z' \to \mu^+\mu^-)$ is first determined using the CL_s procedure described in the previous section.

To convert these cross-section limits into limits on the coupling, Monte Carlo samples are generated for each mediator mass using `MadGraph5_aMC@NLO` [35]. The same generator-level requirements adopted in the signal efficiency determination are applied to ensure consistency between the simulated signal acceptance and the efficiency used in the statistical analysis. The coupling $g_{Z'}$ is then varied while keeping the mediator mass fixed until the predicted production cross section multiplied by the dilepton branching ratio matches the corresponding expected upper limit obtained from the CL_s analysis. Repeating this procedure for all considered mass hypotheses yields the exclusion contour in the $(M_{Z'}, g_{Z'})$ plane.

III. RESULT AND DISCUSSION

The analysis is performed using the CMS Open Data corresponding to the Run G period of the 2016 proton-proton collision dataset at $\sqrt{s} = 13$ TeV. Events are selected from the `DoubleMuon` primary dataset and are required to satisfy at least one double-muon high-level trigger. The trigger menu consists of dimuon triggers requiring two reconstructed muons with transverse momentum thresholds of 17 and 8 GeV, including standard and tracker-muon configurations, variants requiring compatibility with a common longitudinal interaction vertex (Δz), and isolated dimuon triggers for the leading muon within $|\eta| < 2.1$. Since the offline analysis requires both muons to satisfy $p_T > 25$ GeV, the selected events are well within the trigger efficiency plateau. For each event, a unique dimuon candidate is constructed from the reconstructed muons. The muon with the highest transverse momentum satisfying $p_T > 25$ GeV and $|\eta| < 2.4$ is identified as the leading muon. Among the remaining reconstructed muons, the highest-p_T muon with opposite electric charge satisfying the same kinematic requirements is selected as the second muon. Events for which no such opposite-sign partner exists are rejected. Consequently, exactly one dimuon candidate is retained per event, avoiding multiple entries from events containing more than two reconstructed muons.

The selected dimuon candidate is subsequently required to satisfy an invariant mass of $m_{\mu\mu} > 50$ GeV. To ensure a high-purity sample of promptly produced muons, both muons are required to satisfy the CMS medium muon identification working point, together with the impact parameter requirements $|d_{xy}| < 0.05$ cm and $|d_z| < 0.10$ cm. The muon identification, impact parameter, and isolation requirements are based on the CMS prescription described in Ref. [36]. Backgrounds from nonprompt muons originating from heavy-flavor decays and hadronic activity are further suppressed by requiring both muons to satisfy the particle-flow relative isolation criterion $I_{\mathrm{rel}}^{0.4} < 0.15$. The complete set of offline event selection requirements, including the kinematic acceptance, invariant mass requirement, muon identification criteria, impact parameter cuts, isolation requirement, and transverse momentum threshold, are summarized in Table I.

The two-dimensional event distribution in the (m, t) plane exhibits the expected structure associated with the time-dependent normalization function incorporated into the likelihood model. As shown in Fig. 5, the observed variations in event density primarily reflect changes in the data-taking conditions, including variations in luminosity and run duration, rather than genuine physical modulations. These temporal features are well reproduced by the background model, demonstrating that the normalization function provides an adequate description of the time dependence of the dataset. The excellent agreement between the observed data and the background prediction therefore validates the treatment of detector acceptance and data-taking conditions adopted in the time-dependent likelihood analysis.

As shown in Fig. 6, the expected signal production rate decreases rapidly with increasing mediator mass owing to

TABLE I. Summary of the trigger requirements and offline event selection used in the analysis.

Category	Requirement
Invariant mass	$m_{\mu\mu} > 50$ GeV
Muon identification	Both muons satisfy the CMS medium identification working point.
Muon acceptance	Both muons satisfy $\|\eta\| < 2.4$.
Transverse momentum	Both muons satisfy $p_T > 25$ GeV.
Transverse impact parameter	Both muons satisfy $\|d_{xy}\| < 0.05$ cm.
Longitudinal impact parameter	Both muons satisfy $\|d_z\| < 0.10$ cm.
Muon isolation	Both muons satisfy the particle-flow relative isolation requirement $I_{\mathrm{rel}}^{0.4} < 0.15$.

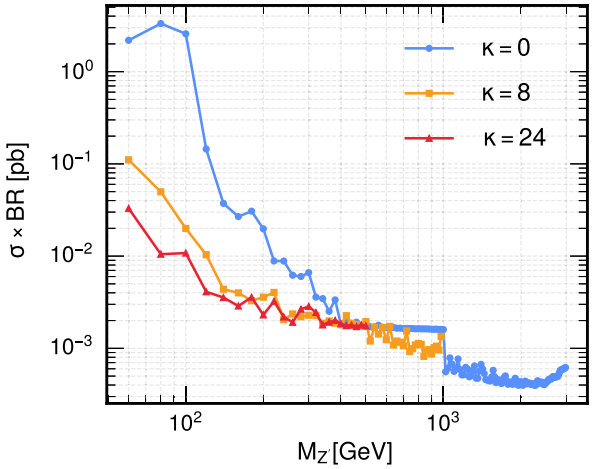


FIG. 6. Expected cross section times branching ratio as a function of the mediator mass for different values of the modulation parameter κ. The signal rate decreases rapidly with increasing mass.

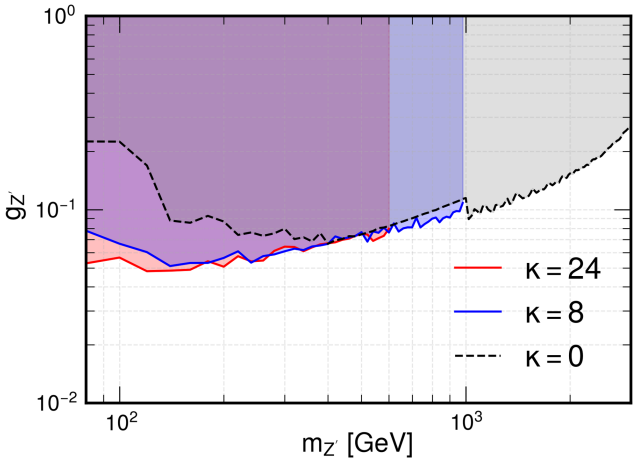


FIG. 7. Upper limits on the coupling $g_{Z'}$ as a function of the mediator mass $m_{Z'}$ for different values of the modulation parameter κ. The dashed curve corresponds to the time-independent case ($\kappa = 0$), while solid curves show the time-dependent results.

the falling production cross section. Consequently, the number of expected signal events decreases, reducing the statistical sensitivity of the search in the high-mass region. This trend is reflected in the expected upper limits on $\sigma \times \mathrm{BR}$ for all values of κ, although the time-dependent scenarios consistently retain improved sensitivity relative to the time-independent case ($\kappa = 0$).

The observed improvement in sensitivity can be understood from the properties of the signal model. As illustrated in Fig. 3, a nonzero modulation amplitude ($\kappa > 0$) gives rise to a characteristic double-peaked time-integrated signal distribution. As the modulation amplitude increases, the separation between the two peaks becomes larger, shifting the upper peak toward higher invariant masses where the smoothly falling Drell-Yan background is substantially reduced. Consequently, a larger fraction of the signal populates a region with a more favorable signal-to-background ratio. At the same time, larger values of κ produce a more pronounced time-dependent structure in the two-dimensional (m, t) space, providing additional discriminating information beyond that available from the invariant-mass distribution alone. The two-dimensional likelihood is therefore able to exploit both the modified signal shape and the temporal information to improve the separation between the signal and the Standard Model background, resulting in enhanced sensitivity without requiring an increase in the total number of signal events.

The agreement between the observed data and the background model in the (m, t) plane indicates that no statistically significant deviation from the SM expectation is observed for any of the benchmark time-dependent signal hypotheses considered in this work. Consequently, the data are found to be consistent with the background-only hypothesis, and 95% CL upper limits are derived on the signal production cross section times branching ratio and the corresponding gauge coupling. The resulting exclusion limits on $g_{Z'}$ are shown in Fig. 7, where the time-independent scenario ($\kappa = 0$) is represented by the dashed curve and the time-dependent cases with $\kappa = 8$ and $\kappa = 24$ by the solid curves. A clear and systematic improvement in sensitivity is observed as the modulation amplitude increases, allowing progressively smaller couplings to be excluded for a fixed mediator mass. At higher mediator masses, the limits become weaker for all values of κ, primarily because the rapidly decreasing production cross section reduces the available signal statistics. Consequently, the separation between the different κ scenarios gradually decreases in the high-mass region. Nevertheless, even with the limited integrated luminosity of the CMS Run G Open Data, the present analysis demonstrates that time-domain resonance searches using event-by-event timing information are experimentally feasible. The sensitivity of this approach is expected to improve with larger datasets, particularly in the high-mass region where the current reach is primarily limited by statistical precision. Cosmological and astrophysical constraints on the underlying time-dependent dark-sector scenario have not been investigated in this work and provide an interesting direction for future study.

IV. SUMMARY AND CONCLUSION

In this work, we have developed a time-dependent search strategy for vector mediators whose masses are modulated by a coherently oscillating ultralight scalar dark matter field. As a benchmark scenario, we considered a Z' gauge boson arising from a gauged $U(1)_{B-L}$ extension of the SM, in which the interaction with the scalar field induces a periodic variation of the effective mediator mass. Unlike conventional resonance searches that rely solely on the

invariant-mass spectrum, such a signal produces a characteristic trajectory in the joint invariant mass-time (m, t) space, providing an additional observable that can be exploited in the statistical analysis.

To capture this distinctive signature, we constructed a two-dimensional extended unbinned likelihood in invariant mass and event time and applied the method to dimuon events from the CMS Run G Open Data corresponding to an integrated luminosity of 7.54 fb^{-1} at $\sqrt{s} = 13$ TeV. A data-driven background model, together with a time-dependent acceptance function derived from the observed Z-boson yield, was used to account for variations in detector conditions and instantaneous luminosity throughout the data-taking period. No statistically significant deviation from the SM expectation was observed, and upper limits at the 95% CL were established on the production cross section times branching ratio and the corresponding gauge coupling.

The resulting exclusion limits demonstrate that incorporating temporal information systematically improves the sensitivity relative to the time-independent scenario ($\kappa = 0$). This improvement can be understood from the properties of the signal model. As the modulation amplitude increases, the time-integrated signal distribution develops enhanced probability density near the turning points of the oscillation, shifting a larger fraction of the signal toward higher invariant masses where the smoothly falling Drell-Yan background provides a more favorable signal-to-background ratio. At the same time, the periodic modulation gives rise to a characteristic correlation between invariant mass and event time that is absent in the Standard Model background, providing additional discriminating information beyond that contained in the invariant-mass distribution alone. Consequently, the greatest improvement is achieved in the low- and intermediate-mass regions, whereas at higher masses the sensitivity becomes increasingly limited by the rapidly decreasing signal yield and the corresponding statistical uncertainty.

Overall, this work establishes a framework for incorporating event time as an additional observable in collider searches for time-dependent new physics. Although demonstrated here for a time-varying Z' boson using a subset of CMS Open Data, the methodology is formulated at the level of collider observables and is readily applicable to a broader class of scenarios involving time-dependent mediator properties. Future analyses using larger datasets and higher integrated luminosities are expected to further extend the discovery potential of this approach.

ACKNOWLEDGMENTS

The authors would like to acknowledge the Department of Science and Technology–Advanced Science and Technology Institute (DOST–ASTI) for providing access to the High-Performance Computing (HPC) resources used in this work. We also gratefully acknowledge the Department of Science and Technology–Accelerated Science and Technology Human Resource Development Program (DOST–ASTHRDP) for scholarship support. The authors sincerely thank Dr. Camille Normand and Dr. Kostantinos Petridis of the University of Bristol for their guidance and valuable discussions during the development and implementation of the time-dependent analysis methodology that formed the basis of this work. In addition, we acknowledge the CMS Collaboration for making the CMS Open Data publicly available, which enabled this study.

DATA AVAILABILITY

The data underlying this study are publicly available through the CMS Open Data portal. The analysis was performed using CMS Run G proton-proton collision data at center of mass energy of 13 TeV, which can be accessed from the CMS Open Data repository. Derived datasets and analysis code used to generate the results presented in this work are available from the corresponding author upon reasonable request.

[1] P. Hernandez, Neutrino physics, CERN Yellow Rep. Sch. Proc. **1**, 139 (2025).
[2] M. B. Hindmarsh, M. Lüben, J. Lumma, and M. Pauly, Phase transitions in the early universe, SciPost Phys. Lect. Notes **24**, 1 (2021).
[3] C. Balázs, A. Mazumdar, E. Pukartas, and G. White, Baryogenesis, dark matter and inflation in the Next-to-Minimal Supersymmetric Standard Model, J. High Energy Phys. 01 (2014) 073.
[4] V. Trimble, Existence and nature of dark matter in the universe, Annu. Rev. Astron. Astrophys. **25**, 425 (1987).
[5] S. Schael *et al.* (ALEPH, DELPHI, L3, OPAL, LEP Electroweak Collaborations), Electroweak measurements in electron-positron collisions at W-Boson-pair energies at LEP, Phys. Rep. **532**, 119 (2013).
[6] G. Cacciapaglia, C. Csaki, G. Marandella, and A. Strumia, The minimal set of electroweak precision parameters, Phys. Rev. D **74**, 033011 (2006).
[7] A. Das, P. S. B. Dev, Y. Hosotani, and S. Mandal, Probing the minimal $U(1)_X$ model at future electron-positron colliders via fermion pair-production channels, Phys. Rev. D **105**, 115030 (2022).

[8] H. Merkel *et al.* (A1 Collaboration), Search for light gauge bosons of the dark sector at the Mainz Microtron, Phys. Rev. Lett. **106**, 251802 (2011).

[9] D. Banerjee *et al.* (NA64 Collaboration), Improved limits on a hypothetical $X(16.7)$ boson and a dark photon decaying into e^+e^- pairs, Phys. Rev. D **101**, 071101 (2020).

[10] D. Banerjee *et al.* (NA64 Collaboration), Search for vector mediator of dark matter production in invisible decay mode, Phys. Rev. D **97**, 072002 (2018).

[11] A. Anastasi *et al.* (KLOE-2 Collaboration), Limit on the production of a new vector boson in $e^+e^- \to U\gamma$, $U \to \pi^+\pi^-$ with the KLOE experiment, Phys. Lett. B **757**, 356 (2016).

[12] S. Abrahamyan *et al.* (APEX Collaboration), Search for a new gauge boson in electron-nucleus fixed-target scattering by the APEX experiment, Phys. Rev. Lett. **107**, 191804 (2011).

[13] R. Essig, P. Schuster, N. Toro, and B. Wojtsekhowski, An electron fixed target experiment to search for a new vector boson A' decaying to e^+e^-, J. High Energy Phys. 02 (2011) 009.

[14] M. Freytsis, G. Ovanesyan, and J. Thaler, Dark force detection in low energy e^-p collisions, J. High Energy Phys. 01 (2010) 111.

[15] J. P. Lees *et al.* (*BABAR* Collaboration), Search for a dark photon in e^+e^- collisions at *BABAR*, Phys. Rev. Lett. **113**, 201801 (2014).

[16] M. Ablikim *et al.* (BESIII Collaboration), Dark photon search in the mass range Between 1.5 and 3.4 GeV/c^2, Phys. Lett. B **774**, 252 (2017).

[17] R. Aaij *et al.* (LHCb Collaboration), Search for dark photons produced in 13 TeV pp Collisions, Phys. Rev. Lett. **120**, 061801 (2018).

[18] F. Wilczek, Problem of strong P and T invariance in the presence of instantons, Phys. Rev. Lett. **40**, 279 (1978).

[19] J. Preskill, M. B. Wise, and F. Wilczek, Cosmology of the invisible axion, Phys. Lett. **120B**, 127 (1983).

[20] L. F. Abbott and P. Sikivie, A cosmological bound on the invisible axion, Phys. Lett. **120B**, 133 (1983).

[21] S. Dodelson and L. M. Widrow, Sterile-neutrinos as dark matter, Phys. Rev. Lett. **72**, 17 (1994).

[22] N. Arkani-Hamed, D. P. Finkbeiner, T. R. Slatyer, and N. Weiner, A theory of dark matter, Phys. Rev. D **79**, 015014 (2009).

[23] D. F. J. Kimball and K. van Bibber edited by, *The Search for Ultralight Bosonic Dark Matter* (Springer, New York, 2023).

[24] J. Guo, Y. He, J. Liu, X.-P. Wang, and K.-P. Xie, Unveiling time-varying signals of ultralight bosonic dark matter at collider and beam dump experiments, Commun. Phys. **6**, 225 (2023).

[25] M. Bauer and S. Chakraborti, Oscillating resonances: Imprints of ultralight dark matter at colliders, arXiv: 2601.19844.

[26] M. H. Fieg, P. J. Fox, J. Zhang, A. Ghosh, V. Varada, and D. Whiteson, Time-dependent signals of new physics at the LHC, arXiv:2605.11071.

[27] L. Basso, A. Belyaev, S. Moretti, G. M. Pruna, and C. H. Shepherd-Themistocleous, Z' discovery potential at the LHC in the minimal $B-L$ extension of the Standard Model, Eur. Phys. J. C **71**, 1613 (2011).

[28] L. Basso, A. Belyaev, S. Moretti, and C. H. Shepherd-Themistocleous, Phenomenology of the minimal B-L extension of the Standard Model: Z' and neutrinos, Phys. Rev. D **80**, 055030 (2009).

[29] L. Basso, S. Moretti, and G. M. Pruna, A renormalisation group equation study of the scalar sector of the minimal B-L extension of the standard model, Phys. Rev. D **82**, 055018 (2010).

[30] CMS Collaboration, DoubleMuon primary dataset in MINIAOD format from Run G of 2016, CERN Open Data Portal (2024), 10.7483/OPENDATA. CMS.UWT2.-PUOE.

[31] CMS Collaboration, DoubleMuon primary dataset in NANOAOD format from Run G of 2016, CERN Open Data Portal (2024), 10.7483/OPENDATA.CMS.ZQS3.LGLP

[32] CMS Collaboration, Simulated dataset ZToMuMu M-50To120 TuneCP5 13 TeV powheg pythia8 in NANOAODSIM format for 2016 collision data, CERN Open Data Portal (2024) 10.7483/OPENDATA.CMS.7SI8.25EU

[33] G. Cowan, K. Cranmer, E. Gross, and O. Vitells, Asymptotic formulae for likelihood-based tests of new physics, Eur. Phys. J. C **71**, 1554 (2011); **73**, 2501(E) (2013).

[34] L. Moneta, K. Belasco, K. S. Cranmer, S. Kreiss, A. Lazzaro, D. Piparo, G. Schott, W. Verkerke, and M. Wolf, The RooStats Project, Proc. Sci. ACAT2010 (**2010**) 057. [arXiv:1009.1003].

[35] J. Alwall, R. Frederix, S. Frixione, V. Hirschi, F. Maltoni, O. Mattelaer, H. S. Shao, T. Stelzer, P. Torrielli, and M. Zaro, The automated computation of tree-level and next-to-leading order differential cross sections, and their matching to parton shower simulations, J. High Energy Phys. 07 (2014) 079.

[36] A. Hayrapetyan *et al.* (CMS Collaboration), Muon identification using multivariate techniques in the CMS experiment in proton-proton collisions at $\sqrt{(s)} = 13$TeV, J. Instrum. **19**, P02031 (2024).